AIAA JOURNAL
Vol. 46, No. 3, March 2008

Dynamics of Composite Aircraft Wings Carrying External Stores

Liviu Librescu*
Virginia Polytechnic Institute and State University, Blacksburg, Virginia 24061
and
Ohseop Song†
Chungnam National University, Daejeon, 305-764, Republic of Korea

DOI: 10.2514/1.25541

This paper focuses on the free vibration and dynamic response to external time-dependent loads of aircraft wings modeled as thin-walled anisotropic composite beams carrying eccentrically located heavy stores. In this context, bending–twisting coupling induced by both the eccentric heavy stores arbitrarily located along the wing span and chord and by the anisotropy of the constituent material that is essential when dealing with aircraft wing problems was included in the approach of the problem. In addition to the anisotropy of constituent materials, transverse shear and warping restraint effects were also incorporated. The governing equations of the wing-store system and the related boundary conditions are derived via Hamilton's principle. To solve the eigenvalue/boundary problems, the extended Galerkin method is applied. Numerical simulations highlighting the implications of external stores coupled with the implementation of the structural tailoring on eigenfrequency and dynamic response to external time-dependent loads are supplied and pertinent conclusions are outlined.

Nomenclature

a_{ij}	=	one-dimensional global stiffness coefficients
b_i	=	mass terms
$J_i^{xx}, J_i^{yy}, J_i^{zz}$	=	ith store's mass moment of inertia about x_i, y_i, and z_i, respectively, taken in the numerical simulations to be nondimensional
L	=	wing semispan
$m_i, \bar{m}_i$	=	mass of the ith store and its dimensionless ($\equiv m_i/m_w$) counterpart
$r_i, \bar{r}_i$	=	offset between the centroid of the ith store and the central line of the clean wing and its dimensionless ($\equiv r_i/L$) counterpart, respectively, positive forward
u_o, v_0, w_o	=	displacements in the X, Y and Z directions, respectively
X, Y, Z	=	global coordinate system
x_i, y_i, z_i	=	local coordinate system associated with the store's centroid, $i = \overline{1, n}$
Z_i, η_i	=	ith mass location along the wing span and its dimensionless ($\equiv Z_i/L$) counterpart, respectively
δ_D, δ	=	Dirac delta function and the variation operator, respectively
θ	=	ply angle
θ_X, θ_Y, ϕ	=	elastic rotations about the X and Y axes and the twisting (positive nose-up) about the Z axis
ω_i, ϖ_i	=	eigenfrequencies and their dimensionless counterparts (ω_i/ω_0), respectively, where $\omega_0 =$ 25.045 rad/s is the fundamental eigenfrequency corresponding to the clean wing and $\theta = 0$ deg

Received 31 May 2006; revision received 20 June 2007; accepted for publication 30 July 2007.

*Professor (deceased, 16 April 2007), Engineering Science and Mechanics Department.
†Professor Mechanical Engineering Department; songos@cnu.ac.kr (Corresponding Author).

Introduction

AIRCRAFT wings, both civil and military, are designed to carry heavy external stores along the wing span and chord. Although the stores in military aircraft are usually associated with fuel tanks and missiles, in transport aircraft the stores consist of large and heavy engines, fuel tanks, or tip stores such as winglets. Depending on their size and location, drastic changes of natural frequencies, dynamic response to time-dependent external excitation, and flutter instability can occur. To achieve a reliable design, a good understanding of their implications is required. To this end, an encompassing structural model of an advanced wing-store system is needed. In this paper, the clean wing is modeled as a thin-walled composite beam that includes the anisotropy and heterogeneity of its material as well as transverse shear and primary and secondary warping. In this context, specialized wing models have been used: Gern and Librescu [1–3] investigated the aeroelastic instability of aircraft wings carrying external stores and (following the developments carried out by Karpouzian and Librescu [4,5]) modeled the wing as a laminated composite plate beam. In [6–11], various problems related with the modeling, free vibration, dynamic response, and active control of aircraft wings carrying externally mounted stores were addressed, in which the wing was modeled as a thin-walled beam featuring the pure bending motion only. A study based on the same assumptions as in [6–11] was developed in [12] (Chapter 8). In this paper, aircraft wings are modeled as a thin-walled anisotropic composite beam carrying external stores, arbitrarily located along the wing span and chord, and in this context, the free vibration and the dynamic response to time-dependent external excitations are investigated. However, in contrast to what was done in [6–12], herein, a doubly bending–twisting coupling is involved: one elastic (due to the anisotropy of constituent materials of the wing) and the other structural (due to the store offset with respect to the wing's centroidal line).

Kinematics and Assumptions

To reduce the 3-D elasticity problem to an equivalent 1-D problem, the components of the displacement vector are represented as [12–15]

$$u(X, Y, Z; t) = u_o(Z; t) - \underline{Y\phi(Z; t)} \tag{1}$$

$$v(X, Y, Z; t) = \underline{v_o(Z; t) + X\phi(Z; t)} \tag{2}$$

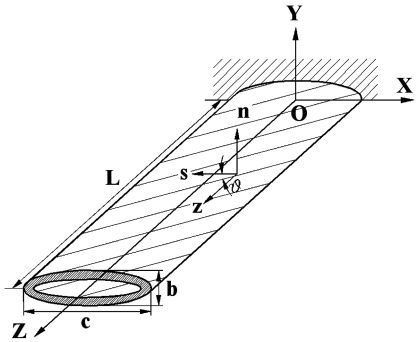

Fig. 1 Thin-walled composite aircraft wing without stores (clean wing): CAS ply-angle configuration.

$$w(X,Y,Z;t) = w_o(Z;t) + \underline{\theta_X(Z;t)}\left[Y(s) - n\frac{\mathrm{d}X}{\mathrm{d}s}\right] + \theta_Y\underline{(Z;t)}\left[X(s) + n\frac{\mathrm{d}Y}{\mathrm{d}s}\right]\underline{-\phi'(Z;t)[F_w(s) + na(s)]} \tag{3}$$

In Eqs. (1–3), as well in some of the next equations, the displacement quantities used in the study are underscored by a solid line. In these equations, u_o, v_0, and w_o denote the rigid-body translations along the X, Y and Z axes, respectively; θ_X, θ_Y, and ϕ denote the rotations about the X and Y axes and the twisting about the Z axis, respectively; and $F_w(s)$ and $na(s)$ play the role of primary and secondary warping functions, respectively. Two sets of coordinate systems are considered: an inertial frame $OXYZ$ with the associated unit vectors $(\mathbf{I}, \mathbf{J}, \mathbf{K})$ (see Fig. 1) and a body-fixed frame $oxyz$ with the associated unit vectors $(\mathbf{i}, \mathbf{j}, \mathbf{k})$ attached to the external stores.

Toward the modeling of the wing-store system, the following assumptions are adopted:

1) The original cross-section of the wing is preserved.

2) Both primary and secondary warping effects are included.

3) Transverse shear effects are incorporated.

4) The constituent material of the structure features anisotropic properties and, in this context, a special layup-inducing transverse shear-transverse bending–twisting elastic coupling is implemented, referred to as a circumferentially asymmetric stiffness configuration (CAS) (see [12–16]).

5) The stores are arbitrarily located along the wing span and chord.

Because the relevant governing equations of motion and the boundary conditions are obtained via Hamilton's principle (HP), the expressions of kinetic energies associated with the external stores, as well as with the clean wings and that of the strain energy, should be provided.

The CAS implies that the ply-angle distribution fulfills the relationships [12–16]

$$\theta(Y) = -\theta(-Y) \tag{4a}$$

$$\theta(X) = -\theta(-X) \tag{4b}$$

where $\boldsymbol{\theta}$ denotes the ply angle that is represented in Fig. 1.

As the results of Eqs. (4) indicate, the flapping–twisting motion that is of primary interest in the present context and involves the variables $v_o(Z;t)$, $\theta_X(Z;t)$, and $\phi(Z;t)$ is exactly decoupled in the governing equations and the associated boundary conditions, from the lagging–extension motion described by the variables $u_o(Z;t)$, $w_o(Z;t)$, and $\theta_Y(Z;t)$. In the kinetic energy, the two motions associated with the flapping–twisting and the lagging–extension also appear to be decoupled. However, in the kinetic energy associated with stores, all the terms (namely, those associated with both bending–twisting and lagging–extension) will be provided.

Kinetic Energies and the Strain Energy of the Clean Wing

To derive the kinetic energies associated with the various components of the system, the unit vectors $(\mathbf{i}, \mathbf{j}, \mathbf{k})$ for the local coordinate system should be expressed in terms of those of the global coordinate system $(\mathbf{I}, \mathbf{J}, \mathbf{K})$. For the linear system, the correlation is [12]

$$\begin{pmatrix}\mathbf{i}\\ \mathbf{j}\\ \mathbf{k}\end{pmatrix} \approx \begin{pmatrix}1 & \phi & \theta_Y\\ \phi & 1 & \theta_X\\ -\theta_Y & -\theta_X & 1\end{pmatrix}\begin{pmatrix}\mathbf{I}\\ \mathbf{J}\\ \mathbf{K}\end{pmatrix} \tag{5}$$

The position vector of an arbitrary point of the ith external store after deformation measured from zero can be expressed as

$$\begin{aligned}\mathbf{R}_i(X,Y,Z;t) &= u_o\mathbf{I} + v_o\mathbf{J} + (w_o + Z_i)\mathbf{K} + (r_i + x_i)\mathbf{i} + y_i\mathbf{j} + z_i\mathbf{k}\\ &= \{u_o + r_i + x_i - \underline{y_i\phi} - z_i\theta_Y\}\mathbf{I}\\ &+ \{\underline{v_0} + \underline{(r_i + x_i)\phi} + y_i - \underline{z_i\theta_X}\}\mathbf{J}\\ &+ \{w_o + Z_i + (r_i + x_i)\theta_Y + \underline{y_i\theta_X} + z_i\}\mathbf{K}\end{aligned} \tag{6}$$

where r_i denotes the offset of the ith external store, measured from its centroid to the centroidal axis of the clean wing, positive forward, and (x_i, y_i, z_i) are the coordinates of points of the ith store. Postulating the symmetry of each individual store, the total kinetic energy of all external stores can be expressed as

$$K_S = \sum_{i=1}^{n} K_i = \sum_{i=1}^{n}\frac{1}{2}[m_i(\dot{u}_o^2 + \underline{\dot{v}_o^2} + \dot{w}_o^2) + \underline{J_i^{xx}\dot{\theta}_X^2} + J_i^{yy}\dot{\theta}_Y^2 + \underline{J_i^{zz}\dot{\phi}^2} + m_i r_i^2(\dot{\theta}_Y^2 + \underline{\dot{\phi}^2}) + 2m_i r_i(\underline{\dot{\phi}\dot{v}_o} + \dot{\theta}_Y\dot{w}_o)]\delta_D(Z - Z_i)\,\mathrm{d}t \tag{7}$$

In these equations, the index $i = \overline{1, n-1}$ refers to the underwing stores, $i = n$ refers to the tip store, m_i and J_i are the mass and the mass moment of inertia of the ith external store, and δ_D denotes Dirac's delta function.

The expressions of kinetic K_w and strain energy U_w of the clean wing, restricted to the CAS configuration, are

$$K_w = \frac{1}{2}\int_0^L [\mathrm{b}_1\dot{\mathrm{v}}_0^2 + (\mathrm{b}_4 + \mathrm{b}_5)\dot{\phi}^2 + (\mathrm{b}_{10} + \mathrm{b}_{18})(\dot{\phi}')^2 + (\mathrm{b}_4 + \mathrm{b}_{14})\dot{\theta}_x^2]\,\mathrm{d}z \tag{8}$$

$$U_w = \frac{1}{2}\int_0^L [\mathrm{a}_{33}(\theta_x')^2 + \mathrm{a}_{55}(\mathrm{v}_0' + \theta_x)^2 + \mathrm{a}_{66}(\phi'')^2 + \mathrm{a}_{77}(\phi')^2 + 2\mathrm{a}_{37}\theta_x'\phi' - 2\mathrm{a}_{56}\varphi''(\mathrm{v}_0' + \theta_x)]\,\mathrm{d}Z \tag{9a}$$

where the work is performed by the distributed external forces

$$\delta W = p_Y(Z,t)\delta v_0(Z,t) + M_x\delta\theta_x(Z,t) + M_Z\delta\phi(Z,t) \tag{9b}$$

In these equations, the a_{ij} and m_{ij} terms are associated with the 1-D stiffness and mass terms, and their expressions can be found in [12].

Governing Equations and Boundary Conditions

Toward the goal of deriving the equations of motion and the associated boundary conditions, HP is used. It may be stated as

$$\delta J = \int_{t_0}^{t_1}(\delta U_w - \delta K_w - \delta K_S - \delta W)\,\mathrm{d}t = 0 \tag{10}$$

To induce the transverse bending–twisting elastic coupling that is beneficial for the response behavior of aircraft wings and to apply the tailoring technique, the *circumferentially asymmetric stiffness configuration* is implemented [12,16] in the present case. Before applying HP to the present problem, we have to properly consider the expressions of

$$\int_{t_0}^{t_1} \delta K_s \, \mathrm{d}t$$

and

$$\int_{t_0}^{t_1} \delta K_w \, \mathrm{d}t$$

in the sense of applying an integration by parts in their expressions and enforcing Hamilton's condition (e.g., see [17]); that is, by considering $\delta V_i = 0$ at $t = t_0, t_1$, where δV_i denotes the variation of any displacement involved in the present problem. As a result, from Eq. (7), we will have

$$\begin{aligned}\int_{t_0}^{t_1} \delta K_S \, \mathrm{d}t = -\int_{t_0}^{t_1} \sum_{i=1}^{n} [\{(m_i \ddot{u}_o)\delta u_o + (\underline{m_i \ddot{v}_o} + \underline{m_i r_i \ddot{\phi}})\delta v_o \\ + (m_i \ddot{w}_o + m_i r_i \ddot{\theta}_Y)\delta w_o + (\underline{J_i^{xx} \ddot{\theta}_X})\delta\theta_X \\ + [m_i r_i \ddot{w}_o + (m_i r_i^2 + J_i^{yy})\ddot{\theta}_Y]\delta\theta_Y \\ + [\underline{m_i r_i \ddot{v}_o} + \underline{(m_i r_i^2 + J_i^{zz})\ddot{\phi}}]\delta\phi\}]\delta_D(Z - Z_i)\, \mathrm{d}t \end{aligned} \tag{11}$$

A similar procedure should be applied, of course, to the variation of the kinetic energy associated with the wing [Eq. (8)].

Inserting Eqs. (8), (9), and (11) in Eq. (10), collecting the terms associated with the same displacement variation, and considering these to be arbitrary and independent, their coefficients in the integrands of Eq. (10) should vanish independently. This yields the governing equations

$$\begin{aligned}\delta v_o\colon\ & -[a_{55}(\theta_X + v_o')]' + (a_{56}\phi'')' + b_1 \ddot{v}_o \\ & + \sum_{i=1}^{n-1} [m_i \ddot{v}_o + m_i r_i \ddot{\phi}]\delta_D(Z - Z_i) = p_Y(Z, t) \end{aligned} \tag{12}$$

$$\begin{aligned}\delta\theta_X\colon\ & -(a_{33}\theta_X')' - (a_{37}\phi')' + a_{55}(\theta_X + v_o') - a_{56}\phi'' \\ & + (b_4 + b_{14})\ddot{\theta}_X + \sum_{i=1}^{n-1} [J_i^{xx}\ddot{\theta}_X]\delta_D(Z - Z_i) = M_X(Z; t) \end{aligned} \tag{13}$$

$$\begin{aligned}\delta\phi\colon\ & (a_{66}\phi'')'' - (a_{77}\phi')' - [a_{56}(\theta_X + v_o')]'' - (a_{73}\theta_X')' \\ & + (b_4 + b_5 + b_{14} + b_{15})\ddot{\phi} - [(b_{10} + b_{18})\ddot{\phi}']' \\ & + \sum_{i=1}^{n-1} [m_i r_i \ddot{v}_o + (m_i r_i^2 + J_i^{zz})\ddot{\phi}]\delta_D(Z - Z_i) = M_Z(Z, t) \end{aligned} \tag{14}$$

and the associated boundary conditions

$$\text{at } Z = 0, \qquad v_o = \theta_X = \phi = \phi' = 0 \tag{15}$$

$$\begin{aligned}&\text{at } Z = L, \\ &\delta v_o\colon\ -a_{55}(\theta_X + v_o') + a_{56}\phi'' - m_n \ddot{v}_o - m_n r_n \ddot{\phi} = 0 \end{aligned} \tag{16}$$

$$\delta\theta_X\colon\ -a_{33}\theta_X' - a_{37}\phi' - J_n^{xx}\ddot{\theta}_X = 0 \tag{17}$$

$$\begin{aligned}\delta\phi\colon\ & (a_{66}\phi'')' - a_{77}\phi' - a_{73}\theta_X' - [a_{56}(v_o' + \theta_X)]' \\ & - (b_{10} + b_{18})\ddot{\phi}' - (m_n r_n^2 + J_n^{zz})\ddot{\phi} - m_n r_n \ddot{v}_o = 0 \end{aligned} \tag{18}$$

$$\delta\phi'\colon\ -a_{56}(v_o' + \theta_X) + a_{66}\phi'' = 0 \tag{19}$$

In Eqs. (12–14), $p_Y(Z, t)$, $M_X(Z, t)$, and $M_Z(Z, t)$ denote the transversal load and the bending and twisting moments about the X and Z axes, respectively.

It can be seen that the boundary conditions at the wing tip ($Z = L$) are affected by the tip store. One should also remark that, consistent with four boundary conditions at the wing root and tip, the governing equation system is of the eighth order. As already indicated, the coefficients a_{ij} and b_i appearing in the preceding equations denote stiffness and inertia quantities, respectively. The stiffness coefficients intervening in the governing equation system and the boundary conditions are the transverse bending stiffness a_{33}, twisting stiffness a_{77}, transverse shear stiffness a_{55} in the Y direction, warping stiffness a_{66}, twist-transverse shear coupling stiffness a_{56}, and bending–twisting cross-coupling stiffness a_{37}. It becomes apparent that these can exhibit a spanwise variation, in the sense of $a_{ij} = a_{ij}(Z)$, and $b_{ij} = b_{ij}(Z)$, and as a result, based on Eqs. (12–19), the case of wings of variable cross sections can be approached.

Time-Dependent External Load

In this paper, the dynamic response to explosive, sonic-boom, and shock-wave types of time-dependent loads will be analyzed (in this sense, see [12]).

In all these cases, the blast wave reaches its peak in such a short time that the structure can be assumed to be loaded instantly. Experimental evidence also suggests that the pressure generated by a blast pulse is uniformly distributed over the beam span. As a result, although for this case M_X and M_Z are zero-valued quantities, the pressure pulse will exhibit only a time dependence.

In the cases of an explosive blast and sonic boom, the overpressures can be expressed in a unified form as

$$p_Y(t) = P_m(1 - t/t_p)[H(t) - \delta_b H(t - rt_p)] \tag{20}$$

where $H(t)$ denotes the Heaviside step function; δ_b is a tracer that takes the values 1 or 0, depending on whether the sonic-boom or the triangular blast is considered, respectively; t_b denotes the positive phase duration of the pulse measured from the time of impact of the structure; and r denotes the shock pulse length factor. For $r = 1$, the sonic boom reduces to a triangular explosive pulse, and for $r = 2$, it corresponds to a symmetric sonic-boom pulse, whereas for $1 < r < 2$, an asymmetric N-shaped pulse results. P_m denotes the peak reflected pressure in excess to the ambient one.

A special case of blast and sonic-boom pulses corresponds to a shock-wave modeled as a step pulse. This case is obtained from Eq. (20) by considering $t_p \to \infty$ and δ_b.

Solution Methodology

Toward the goal of solving the eigenvalue/boundary-value problems (that is, the free vibration and the dynamic-response problem), the following representation of displacement functions is used:

$$\begin{pmatrix} v_o(Z; t) \\ \theta_X(Z; t) \\ \phi(Z; t) \end{pmatrix} = \begin{pmatrix} \boldsymbol{V}^T(Z)\boldsymbol{q}_v(t) \\ \boldsymbol{X}^T(Z)\boldsymbol{q}_x(t) \\ \boldsymbol{\Phi}^T(Z)\boldsymbol{q}_\phi(t) \end{pmatrix} \tag{21}$$

where $\boldsymbol{V}$, $\boldsymbol{X}$, and $\boldsymbol{\Phi}$ are the vectors of trial functions that are chosen to satisfy, as a necessary requirement, the geometric boundary conditions; $\boldsymbol{q}_v$, $\boldsymbol{q}_X$, and $\boldsymbol{q}_\phi$ are the vectors of generalized coordinates; and superscript T denotes transpose operation. For synchronous motion, $\boldsymbol{q}(V) = \boldsymbol{Q}\exp(i\omega t)$, where $\boldsymbol{Q}$ is a constant vector and ω is a constant-valued quantity, both generally complex. Following the usual steps (e.g., see [13]) and discarding the transverse load, one obtains the eigenvalue problem

$$-\omega^2 \boldsymbol{M}\boldsymbol{Q} + \boldsymbol{K}\boldsymbol{Q} = 0 \tag{22}$$

where ω must satisfy the characteristic equation obtained from $\det(\boldsymbol{K}\text{-}\omega^2\ \boldsymbol{M}) = 0$. The matrices of mass $[\boldsymbol{M}]$ and stiffness $[\boldsymbol{K}]$ are displayed in the Appendix. The solution of the system is based on the

Table 1 Material characteristics of the constituent material

$E_1 = 137.919 \times 10^9$ N/m^2	$E_2 = E_3 = 9.654$ N/m^2	
$G_{12} = 5.517 \times 10^9$ N/m^2	$G_{23} = G_{31} = 4.138 \times 10^9$ N/m^2	
$\nu_{21} = \nu_{31} = 0.021$	$\nu_{32} = 0.3$	$\rho = 1528.15$ kg/m^3

Table 2 Characteristics of the time-dependent loads

Dimensionless load amplitude	$p_m = P_m L/a_{55}(0) = 10^{-4}$
Total load over the wing semispan	$P_m L = 7597$ N
Sonic boom	$t_p = 0.25$ s, $r = 1.2$, $p_m = 10^{-4}$
Triangular pulse	$t_p = 0.3$ s, $p_m = 10^{-4}$
Step loading	$p_m = 10^{-4}$

extended Galerkin method (EGM), in which context polynomials in the Z coordinate are used as trial functions. By using this method, the discretized equation for the dynamic response is

$$\boldsymbol{M}\,\ddot{\mathbf{q}} + \boldsymbol{K}\mathbf{q} = \boldsymbol{F} \tag{23}$$

where $\boldsymbol{F}$ denotes the external force vector. Multiplying the preceding equation by $\boldsymbol{M}^{-1}$, introducing the generalized velocities $\dot{\boldsymbol{q}}$ as an auxiliary variable by means of the matrix identity $\dot{\boldsymbol{q}} - \dot{\boldsymbol{q}} = 0$, and defining the state-space vector

$$\boldsymbol{X} = \begin{pmatrix} \boldsymbol{q} \\ \dot{\boldsymbol{q}} \end{pmatrix} \tag{24}$$

Eq. (24) can be converted to state-space form as

$$\dot{\boldsymbol{X}}(t) = \boldsymbol{A}\boldsymbol{X}(t) + \boldsymbol{B}\boldsymbol{F}(t) \tag{25}$$

The solution of Eq. (26), providing the dynamic response, was carried out via the transition matrix procedure in discrete time. In continuous time representation, its solution is

$$\boldsymbol{X}(t) = \boldsymbol{\Lambda}(t)\boldsymbol{X_0} + \int_0^t \Lambda(\mathrm{t} - \tau)\boldsymbol{B}\boldsymbol{F}(\tau)\,\mathrm{d}\tau \tag{26}$$

where $\boldsymbol{\Lambda}(t) \equiv \exp \boldsymbol{A}(t)$.

In the present numerical simulations, $\boldsymbol{X}_0$ $[\equiv \boldsymbol{X}(t=0)]$ was considered to be zero.

Numerical Simulations

The numerical simulations involve the behavior of the system from the eigenfrequency and dynamic-response points of view, as affected by the underwing and tip stores, by their location and the ply angles that reflect the directional properties of the constituent material of the aircraft wing. In these numerical results, the wing structure is simulated as a uniform biconvex cross-sectional composite beam, characterized by $c = 1$ m, $L = 6$ m, and $h = 0.01$ m.

We will consider, unless otherwise stated, the case of two stores: $i = 1$ is the underwing store of relative mass $\bar{m}_1 = 0.5$, $\bar{r}_1 = 0.05$, $J_1^{xx} = 0.01$, and $J_1^{zz} = 0.02$, and $i = 2$ is the tip store characterized by $\bar{m}_T = 0.2$, $\bar{r}_T = 0.05$, $J_T^{xx} = 0.0051$, and $J_T^{zz} = 0.01$.

The material properties of the wing structure correspond to T300/5028 graphite/epoxy, as provided in Table 1.

The external time-dependent loads used in the dynamic-response analysis consist of an explosive triangular pulse, sonic boom, and step loadings. Their characteristics are provided in Table 2.

As is clearly seen, the dimensionless load amplitude p_m was selected to be the same for all considered cases, where $a_{55}(0)$ denotes the stiffness a_{55} evaluated at $\theta = 0$.

Free Vibration

In the case of free vibration ($p_Y = 0$), a few results that reflect the implication of the underwing and tip stores (as well as their location, considered in conjunction with the ply angle) on various mode eigenfrequencies are supplied.

In Fig. 2, $\mathcal{B}$ and $\mathcal{T}$ identify the pure bending and twisting eigenfrequencies occurring at $\theta = 0$ and 90 deg, for which the bending–twisting coupling stiffness a_{37} vanishes and, as a result, the decoupling bending–twisting occurs. The results show that in the presence of the store, a shift of the eigenfrequency maxima with respect to $\theta = 90$ deg, proper to the case of the clean wing, is experienced. In all cases, a drop of eigenfrequencies is occurring, corresponding to the case of the wing with stores, compared with those of the clean wing. This trend is similar to thos obtained via the finite element method in [18] and in the context of a solid beam model of the wing in [3].

In Figs. 3–7, the first five eigenfrequencies depicted in sequence against the ply angle θ are presented. In all of them, various scenarios are presented, consisting of the clean wing (C), underwing store (U) located at $\eta_1 = 0.5$, tip store (T), and both stores (B).

The results reflect again the eigenfrequency disymmetry with respect to the variation of θ and that the ply angle can constitute a powerful factor toward the increase of eigenfrequencies. They also reveal that the natural frequencies of the wing with underwing and/or tip store are lower than those of the clean-wing counterpart.

The results of Fig. 8 reveal that the tip store results in a larger decrease of eigenfrequencies than in the case of the underwing store, a trend that is exacerbated in the case of higher mode eigenfrequencies. One can also see that beyond a certain value of the store mass that depends on the mode number, the decrease of eigenfrequencies tends to be attenuate.

Figure 9 shows the bending free-vibration behavior ($\theta = 0$ deg) of a wing carrying an underwing store of fixed mass and a tip store. The results reveal again that the eigenfrequencies are lowered by increasing the tip mass. It also clearly emerges that by increasing the

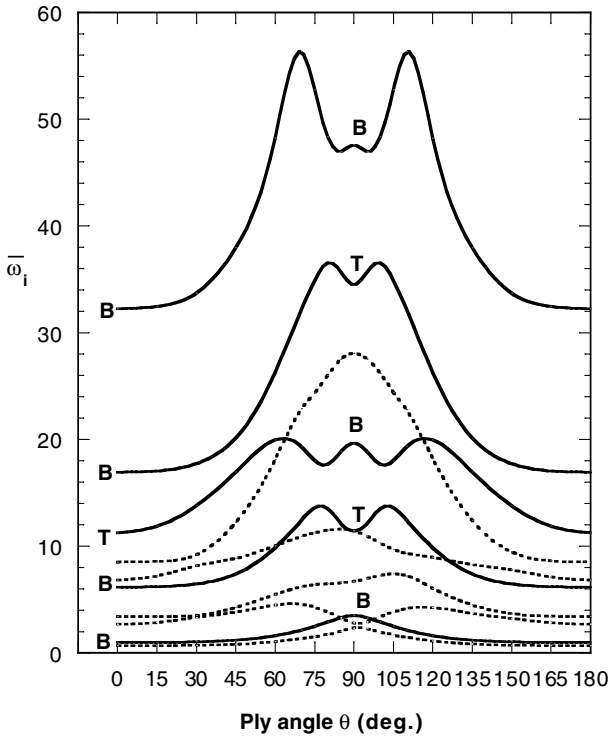

Fig. 2 Lowest five frequencies vs ply angle for a clean wing (solid line) and for the wing with underwing and tip stores (dotted line), $\bar{m}_1 = 0.5$, $\bar{m}_T = 0.2$.

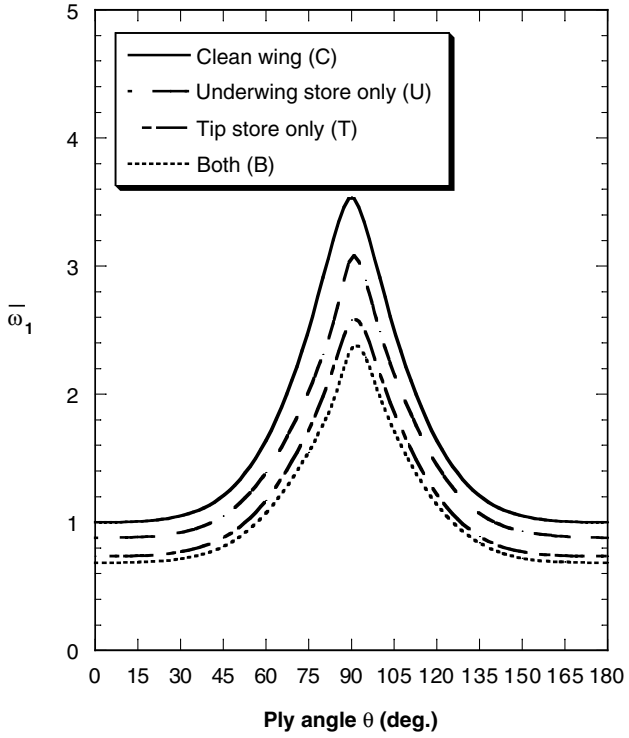

Fig. 3 First eigenfrequency vs ply angle θ.

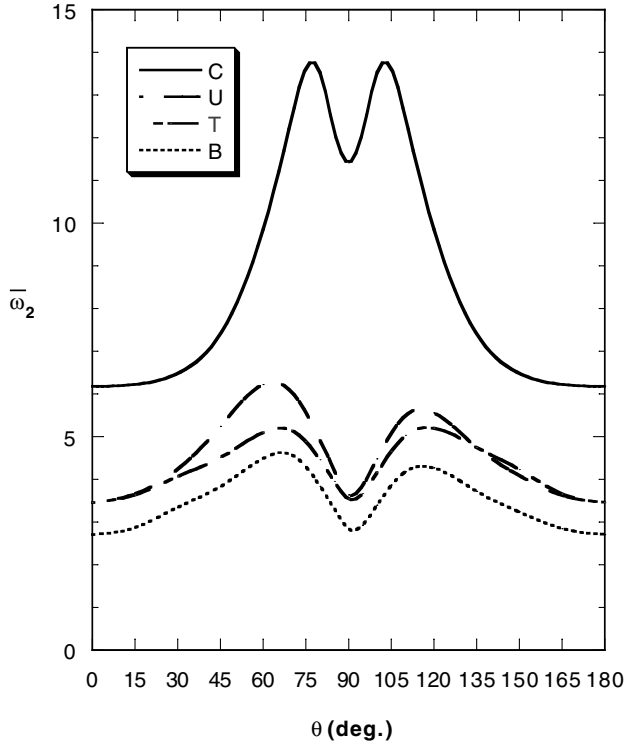

Fig. 4 Second eigenfrequency vs ply angle θ.

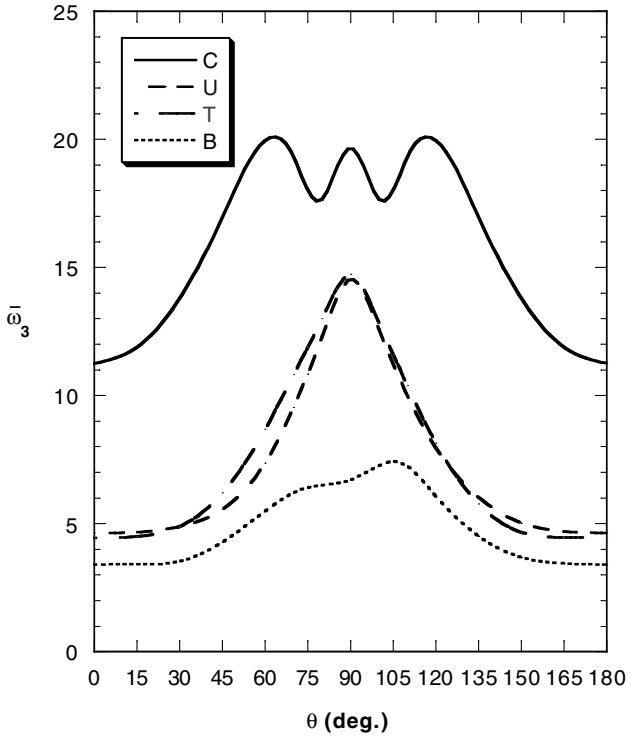

Fig. 5 Third eigenfrequency vs ply angle θ.

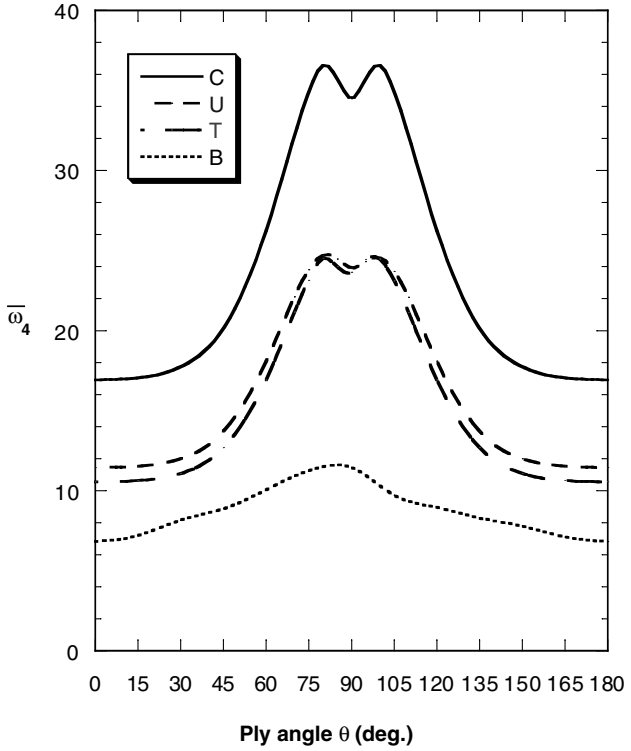

Fig. 6 Fourth eigenfrequency vs ply angle θ.

tip mass, the increase of the second mode eigenfrequency is shifted outward, together with the shift outward of the node line of the second bending mode number. This trend is consistent with that theoretically and experimentally obtained in [3,19], respectively.

Figures 10–12 depict the variations of the first three eigenfrequencies against the aspect ratio of the semiwing L/c for three selected values of θ in both underwing and tip stores.

The displayed results reveal that the increase of the wing aspect ratio results in a decrease of eigenfrequencies, a decrease that is stronger in the case of ply angle $\theta = 90$ deg than for $\theta = 0$ and 45 deg. Moreover, as clearly shown for high-aspect-ratio wings, the higher mode eigenfrequencies of aircraft wings with stores experience a smaller variation with the increase of the ply angle. In other words, for *large-aspect-ratio wings with stores*, the structural tailoring can provide only a modest increase of eigenfrequencies.

Big differences also appear in the eigenmodes of aircraft wings with stores, compared with their clean wing counterparts. In this sense, Figs. 13 and 14, depicting the first three eigenmodes in

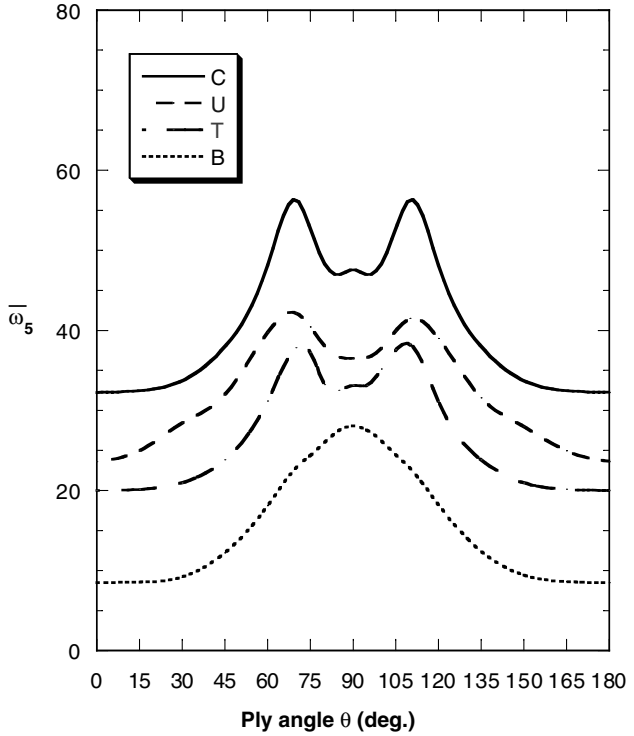

Fig. 7 Fifth eigenfrequency vs ply angle θ.

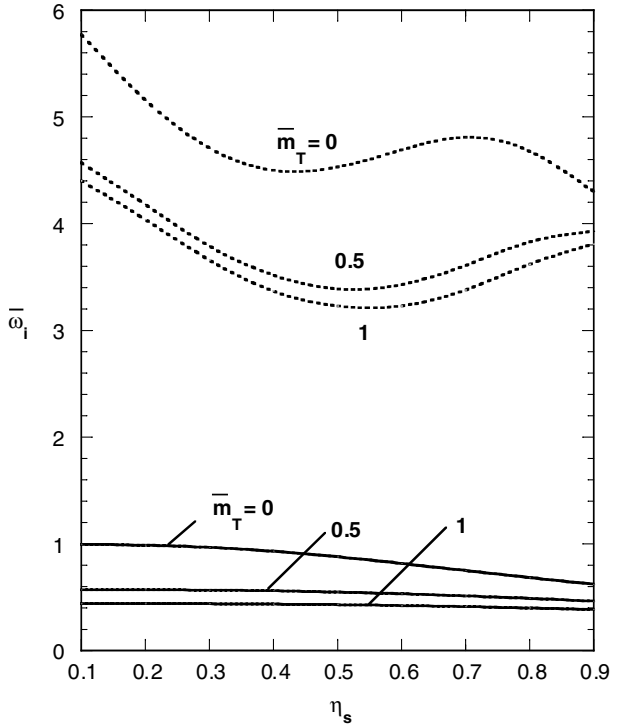

Fig. 9 Influence of dimensionless tip store mass $\bar{m}_T$ and underwing store location on vibration frequencies of the first and second natural bending modes; $\bar{m}_1 = 0.5$ and $\theta = 0$ deg.

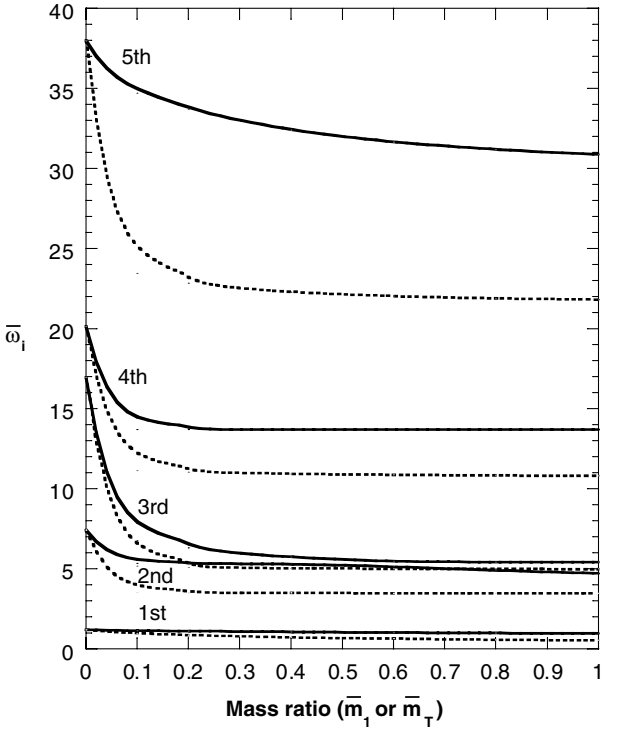

Fig. 8 Variation of the first five eigenfrequencies with store mass; underwing store only (solid line) and tip store only (dotted line); $\theta = 45$ deg.

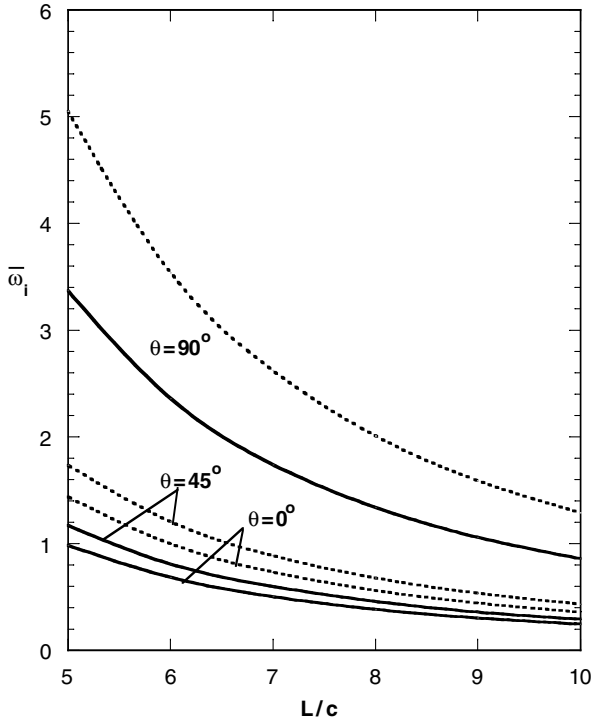

Fig. 10 First eigenfrequency vs aspect ratio L/c for ply angles $\theta = 0$, 45, and 90 deg; clean wing (dotted line) and wing with stores (solid line).

bending and twisting, respectively, reveal the big difference between those of the clean wing and the wing with stores.

Finally, it should also be mentioned that there is a perfect superposition of results between all the findings supplied in [12] (Chapter 8) regarding the variation of bending eigenfrequencies with the location along the wing span of underwing stores of various mass ratios and the counterparts obtained via the specialization of the present structural model. For this reason, these results are not supplied here.

Dynamic Response

The time history is shown in Fig. 15a for the transversal bending amplitude and in Fig. 15b for the twisting amplitude of the wing tip to a sonic-boom pulse in the case of an eccentrically located underwing

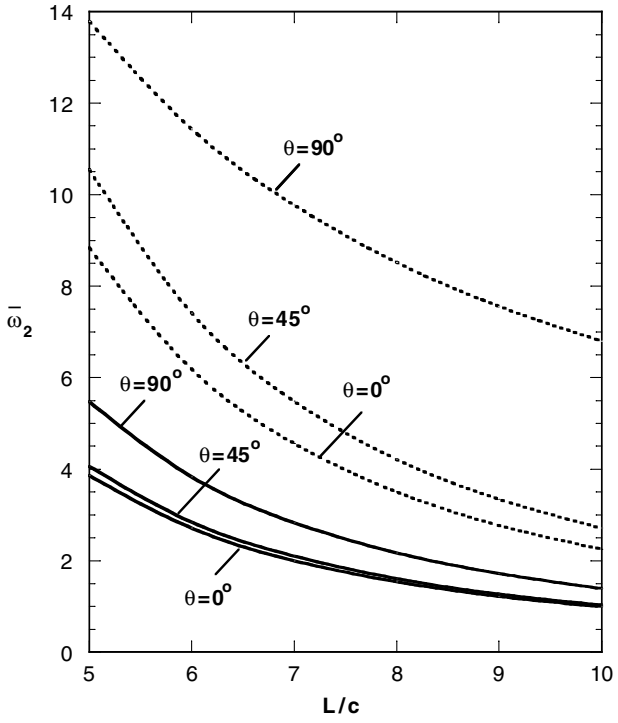

Fig. 11 Counterpart of Fig. 10 for the second eigenfrequency.

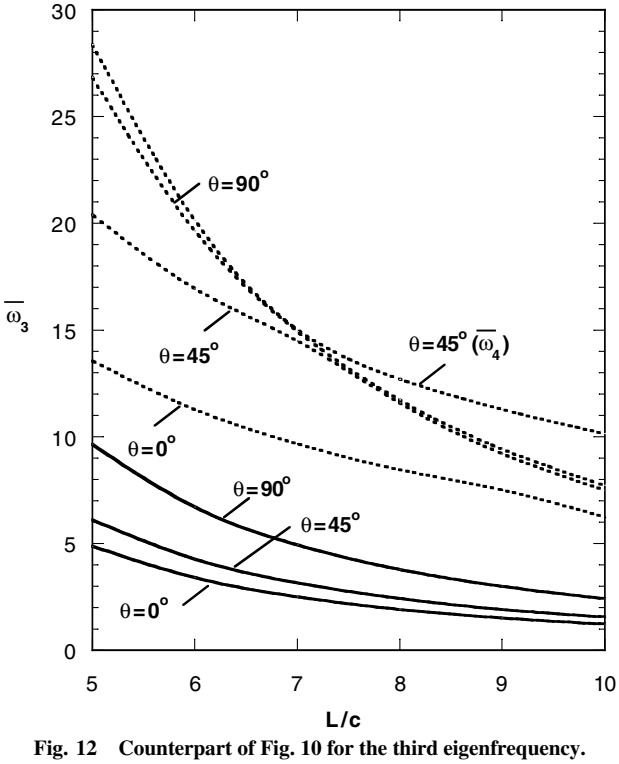

Fig. 12 Counterpart of Fig. 10 for the third eigenfrequency.

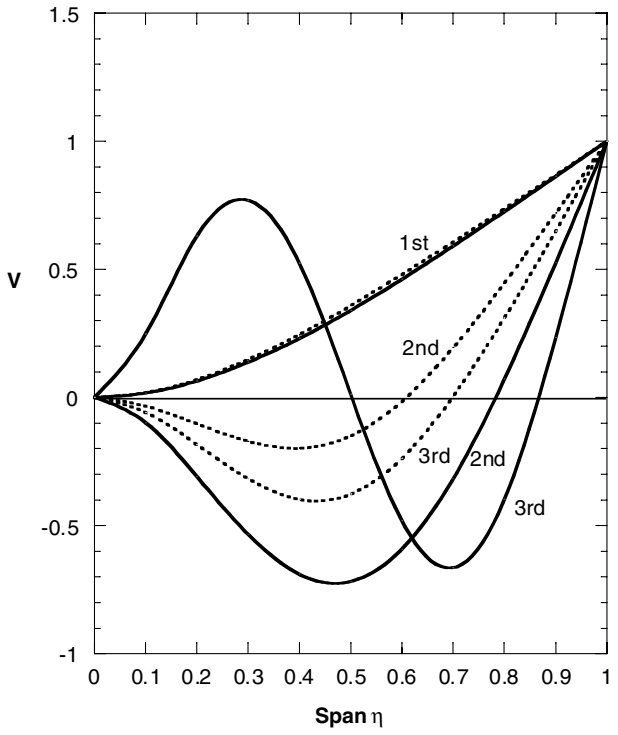

Fig. 13 First three mode shapes associated with v_0; clean wing (solid line) and underwing store only (dotted line); $\bar{m}_1 = 1$ and $\theta = 0$ deg.

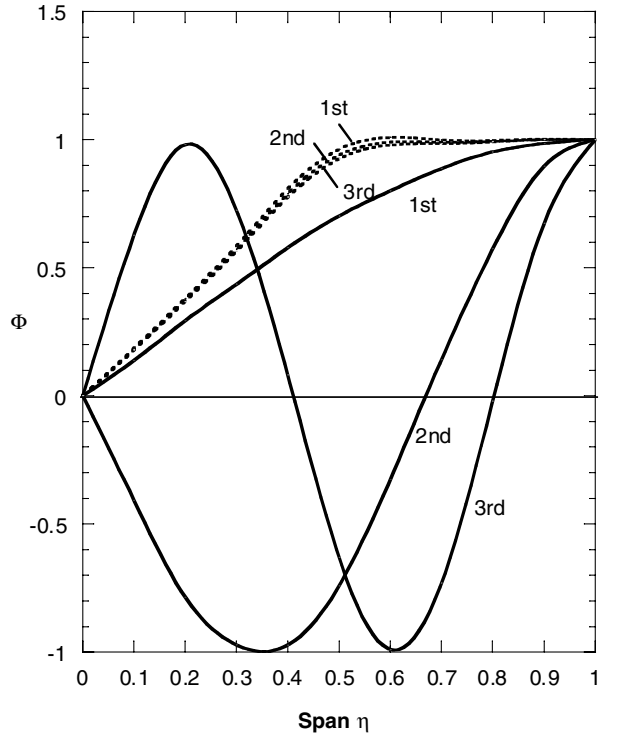

Fig. 14 First three mode shapes associated with ϕ; clean wing (solid line) and underwing store only (dotted line); $\bar{m}_1 = 1$, $\theta = 0$ deg.

store. Although for the bending response, the amplitudes are largest for $\bar{m}_1 = 0.1$ and lowest for $\bar{m}_1 = 0.9$, for the twisting response, the opposite situation takes place. This is especially true due to the fact that for this case ($\theta = 90$ deg), the only source of the bending–twisting coupling is due to the store offset. As a result, with the increase of the store mass, the twisting amplitude also increases.

The dynamic response is considered in Fig. 16a for bending and in Fig. 16b for twisting of the wing tip to a sonic-boom pulse for selected store offsets. Although the effect of the offset on transversal deflection amplitude appears to be immaterial, in the case of the twisting time history for $\bar{r}_1 = -0.2$ and $\bar{r}_1 = 0.2$, the responses exhibit mirror symmetry.

The dynamic response is considered in Fig. 17a for the deflection and in Fig. 17b for the twisting measured at two different spanwise locations ($\eta_1 = 0.5$ and 1) of the wing exposed to a shock-wave modeled as a Heaviside pulse.

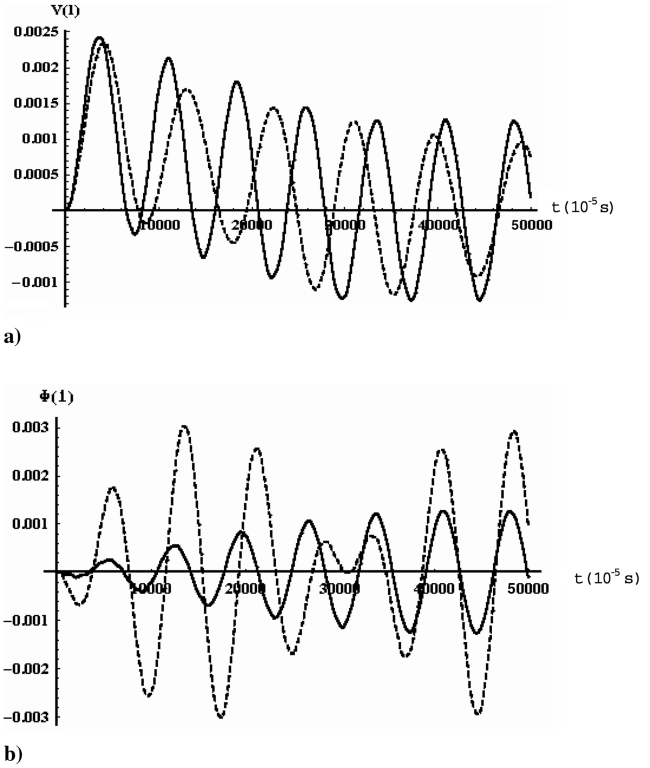

Fig. 15 Deflection and twisting dynamic response at the wing tip to a sonic-boom pulse for $m_1 = 0.1$ (solid line) and $m_1 = 0.9$ (dotted line); $\theta = 90$ deg; underwing store only.

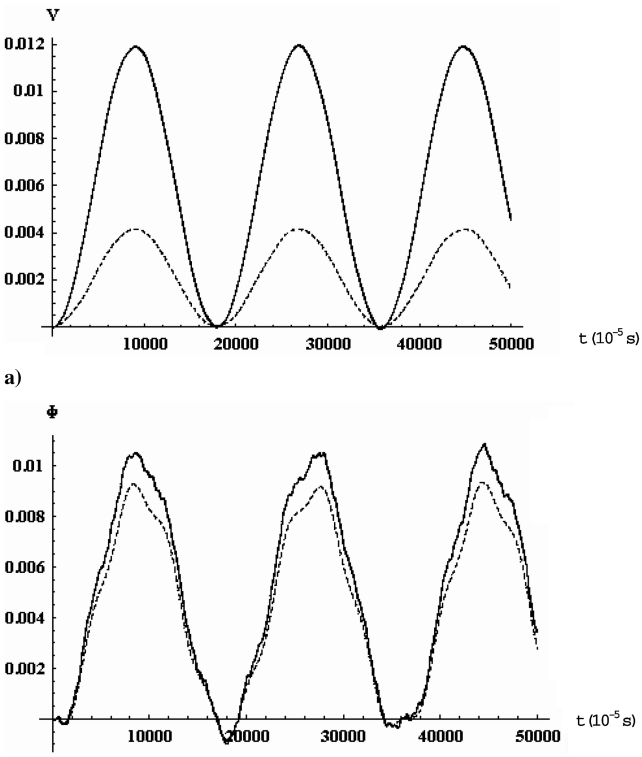

Fig. 17 Time history of a) deflection and b) twisting amplitudes at two different locations; $\eta_1 = 0.5$ (dotted line) and $\eta_1 = 1$ (solid line) to a step pulse; $\theta = 60$ deg; underwing store only.

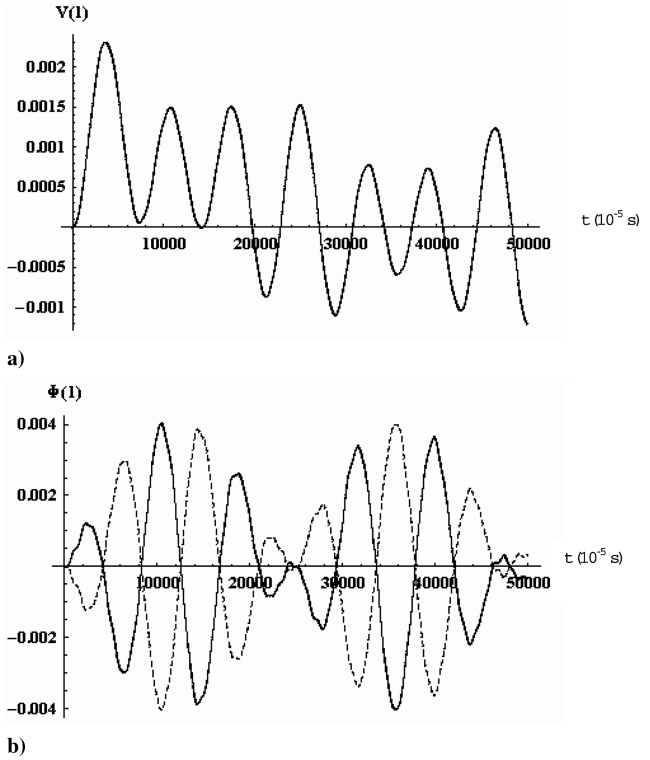

Fig. 16 Deflection and twisting time histories due to a sonic-boom pulse for $\bar{r}_1 = -0.2$ (solid line) and $\bar{r}_1 = 0.2$ (dotted line); underwing store only; $\theta = 90$ deg.

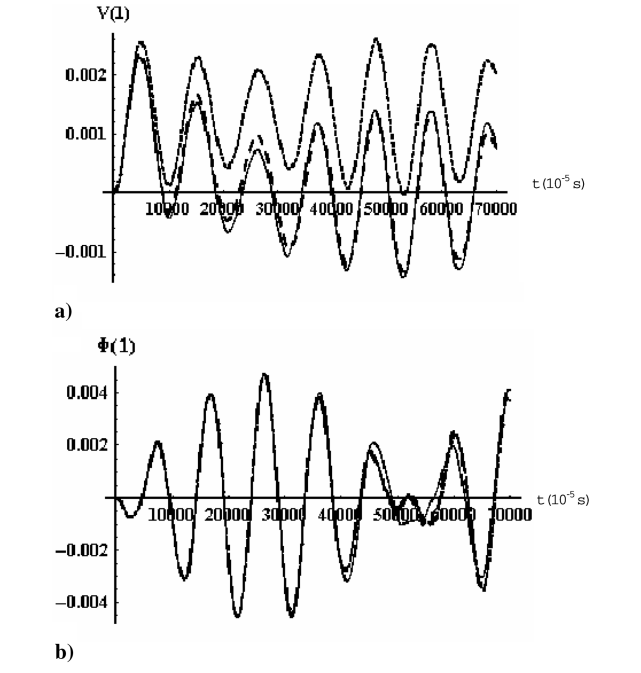

Fig. 18 Deflection and twisting wing tip time histories of three different loading configurations: sonic-boom pulse (solid line), triangular pulse (dashed), and step load (dotted line); $\theta = 90$ deg; with both stores; $m_1 = 0.5$ and $m_T = 0.2$.

For the bending time history, the trend shows that the deflection amplitude at the wing tip is larger than at the midspan. However, keeping in mind that the maximum stiffness in twisting is reached for $\theta = 60$ deg, the twisting amplitudes at these two locations appear to be almost equal.

The time histories are presented in Fig. 18a for bending and in Fig. 18b for twisting of the wing tip to three different dynamic pulses: sonic-boom pulse (solid line), triangular pulse (dashed line), and step pulse (dotted line). The results reveal that for the transversal bending, the step pulse appears to be the most severe among those considered

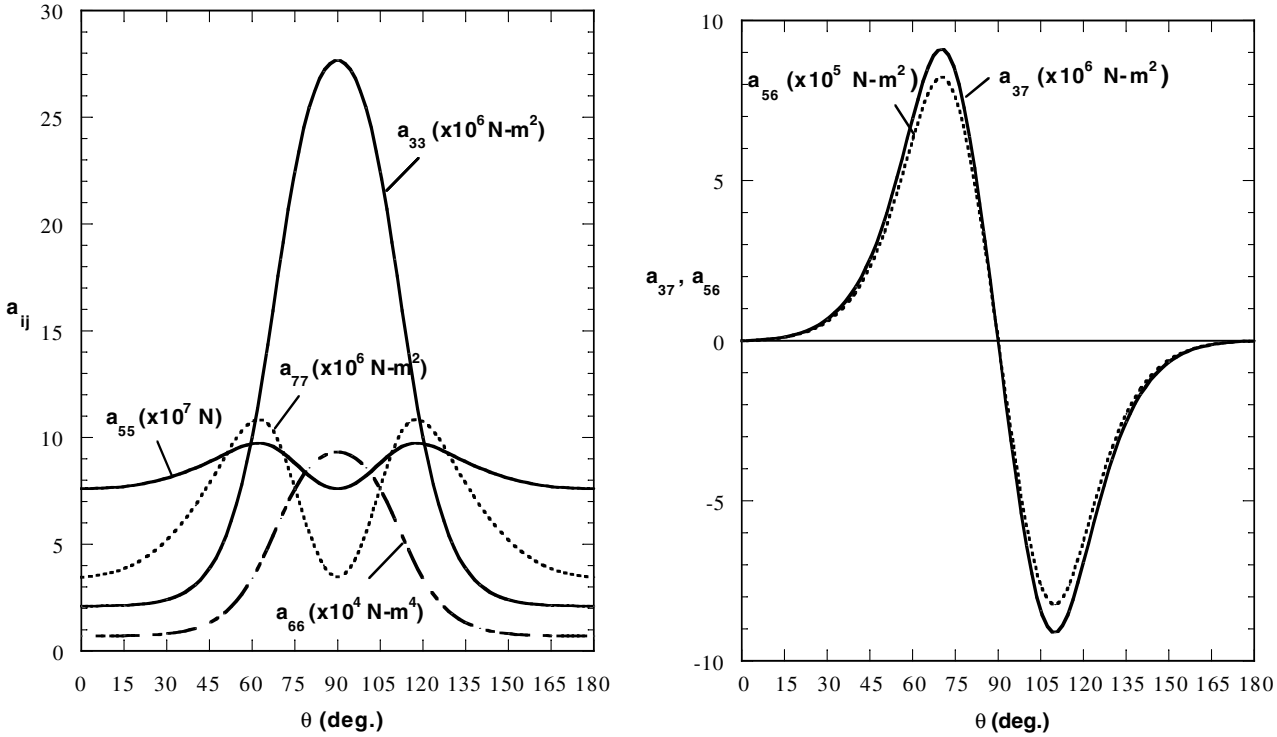

a) b)

Fig. 19 Variation of a number of stiffnesses with ply angle: a) a_{33} (flap bending), a_{55} (shear), a_{77} (torsion), and a_{66} (warping) and b) a_{37} (bending–torsion coupling) and a_{56} (shear-warping coupling) with ply angle θ.

here, in the sense that a maximum deflection amplitude is resulting. At the same time, the sonic-boom and the triangular pulses appear to provide the same deflection amplitude in the free-vibration range. For the twisting dynamic response, keeping in mind that the elastic bending–twisting coupling stiffness a_{37} vanishes for $\theta = 90$ deg, the twisting is generated by the offset of the underwing strip only. In this case, it appears that the twisting amplitude time history does not exhibit any difference with respect to the considered pressure pulse, especially in the forced-motion range.

As evident from the previously displayed results, the variation of the ply angle heavily influences the stiffness quantities and implicitly influences the free vibration and dynamic response of the wing structure.

To get a better understanding of the implications of the ply angle and of the obtained trends, the variations with θ of the basic stiffness quantities a_{37}, a_{77}, a_{33}, a_{55}, and a_{56} are provided in Figs. 19a and 19b.

Before closing this section, it should be stressed that the model of the clean wings considered in this paper was validated in [20] against a large number of theoretical and experimental results, and excellent agreements have been reached.

Conclusions

An encompassing composite structural wing model incorporating a number of nonclassical effects was developed, its capabilities to address eigenvibration and dynamic-response problems were highlighted, and comparisons with some of the available results were indicated.

This structural model can be successfully used to address issues of aeroelastic instability and aeroelastic response.

Appendix: Mass and Stiffness Matrices

The matrices associated with the mass $[M]$ and stiffness $[K]$ intervening in Eqs. (22) and (23) have the following form:

$$[M] = \begin{pmatrix} M_{11} & M_{12} & M_{13} \\ M_{21} & M_{22} & M_{23} \\ M_{31} & M_{32} & M_{33} \end{pmatrix} \tag{A1a}$$

$$[K] = \begin{pmatrix} K_{11} & K_{12} & K_{13} \\ K_{21} & K_{22} & K_{23} \\ K_{31} & K_{32} & K_{33} \end{pmatrix} \tag{A1b}$$

The entries of these two matrices are provided next.

Entries of the mass matrix:

$$M_{11} = \int_0^{\mathrm{L}} \left\{ b_1 VV^T + \sum_{i=1}^{n-1} m_i VV^T \delta_D(Z - Z_i) \right\} \mathrm{d}Z - [m_n VV^T]_{z=L} \tag{A2}$$

$$M_{13} = \int_0^L \left\{ \sum_{i=1}^{n-1} m_i r_i V\Phi^T \delta_D(Z - Z_i) \right\} \mathrm{d}Z - [m_n r_n V\Phi^T]_{Z=L} \tag{A3}$$

$$M_{22} = \int_0^L \left\{ (b_4 + b_{14}) XX^T + \sum_{i=1}^{n-1} J_i^{xx} XX^T \delta_D(Z - Z_i) \right\} \mathrm{d}Z - [J_n^{xx} XX^T]_{Z=L} \tag{A4}$$

$$M_{31} = \int_0^L \left\{ \sum_{i=1}^{n-1} m_i r_i \Phi V^T \delta_D(Z - Z_i) \right\} \mathrm{d}Z - [m_n r_n \Phi V^T]_{Z=L} \tag{A5}$$

$$M_{33} = \int_0^L \left\{ (b_4 + b_5 + b_{14} + b_{15})\Phi\Phi^T + (b_{10} + b_{18})\Phi'\Phi'^T + \sum_{i=1}^{n-1}(m_i r_i^2 + J_i^{zz})\Phi\Phi^T \delta_D(Z - Z_i) \right\} dZ - [(m_n r_n^2 + J_n^{zz})\Phi\Phi^T]_{z=L} \quad \text{(A6)}$$

$$M_{12} = M_{21} = M_{23} = M_{32} = 0 \quad \text{(A7)}$$

Here and in the following equations, the superscript T denotes transpose operation.

Entries of the stiffness matrix:

$$K_{11} = \int_0^L \{a_{55} V' V'^T\}\, dZ \quad \text{(A8)}$$

$$K_{12} = \int_0^L \{a_{55} V' X^T\}\, dZ \quad \text{(A9)}$$

$$K_{13} = \int_0^L \{a_{56} V' \Phi''^T\}\, dZ \quad \text{(A10)}$$

$$K_{21} = \int_0^L \{a_{55} X V'^T\}\, dZ \quad \text{(A11)}$$

$$K_{22} = \int_0^L \{a_{33} X' X'^T + a_{55} X X^T\}\, dZ \quad \text{(A12)}$$

$$K_{23} = \int_0^L (a_{37} + a_{56}) X' \Phi'^T\, dZ - [a_{56} X \Phi'^T]_{Z=L} \quad \text{(A13)}$$

$$K_{31} = -\int_0^L \{a_{56} \Phi V'''^T\}\, dZ + [a_{56} \Phi V''^T - a_{56} \Phi' V'^T]_{Z=L} = -\int_0^L \{a_{56} \Phi'' V'^T\}\, dZ \quad \text{(A14)}$$

$$K_{32} = \int_0^L (a_{37} + a_{56}) \Phi' X'^T\, dZ - [a_{56} \Phi' X^T]_{Z=L} \quad \text{(A15)}$$

$$K_{33} = \int_0^L \{a_{66} \Phi'' \Phi''^T + a_{77} \Phi' \Phi'^T\}\, dZ \quad \text{(A16)}$$

References

[1] Gern, F. H., and Librescu, L., "Static and Dynamic Aeroelasticity of Advanced Aircraft Wings Carrying External Stores," *AIAA Journal*, Vol. 36, No. 7, 1998, pp. 1121–1129.

[2] Gern, F. H., and Librescu, L., "Effects of Externally Mounted Stores on Aeroelasticity of Advanced Swept Cantilevered Aircraft Wings," *Aerospace Science and Technology*, Vol. 2, No. 5, 1998, pp. 321–333.
doi:10.1016/S1270-9638(98)80008-4

[3] Gern, F. H., and Librescu, L., "Aeroelastic Tailoring of Composite Wings Exhibiting Nonclassical Effects and Carrying External Stores," *Journal of Aircraft*, Vol. 37, No. 6, Nov.–Dec. 2000, pp. 1097–1104.

[4] Karpouzian, G., and Librescu, L., "Comprehensive Model of Anisotropic Composite Aircraft Wings Suitable for Aeroelastic Analyses," *Journal of Aircraft*, Vol. 31, No. 3, May–June 1994, pp. 703–712.

[5] Karpouzian, G., and Librescu, L., "Nonclassical Effects on Divergence and Flutter of Anisotropic Swept Aircraft Wings," *AIAA Journal*, Vol. 34, No. 4, Apr. 1996, pp. 786–794.

[6] Song, O., and Librescu, L., "Bending Vibrations of Adaptive Cantilevers with External Stores," *International Journal of Mechanical Sciences*, Vol. 38, No. 5, 1996, pp. 483–498.
doi:10.1016/0020-7403(95)00075-5

[7] Song, O., Librescu, L., and Rogers, C. A., "Adaptive Response Control of Cantilevered Thin-Walled Beams Carrying Heavy Concentrated Masses," *Journal of Intelligent Material Systems and Structures*, Vol. 5, No. 1, 1994, pp. 42–48.
doi:10.1177/1045389X9400500105

[8] Librescu, L., and Song, O., "Static and Dynamic Behavior of Adaptive Aircraft Wings Carrying Externally Mounted Stores," *Structronic Systems: Smart Structures, Devices and Systems*, edited by H. S. Tzou, Series on Stability, Vibration Control of Systems, Vol. 1, World Scientific, Singapore, 1997, pp. 113–138.

[9] Na, S., and Librescu, L., "Dynamic Response of Adaptive Cantilevers Carrying External Stores and Subjected to Blast Loading," *Journal of Sound and Vibration*, Vol. 231, No. 4, 2000, pp. 1039–1055.
doi:10.1006/jsvi.1999.2627

[10] Librescu, L., and Na, S. S., "Vibration and Dynamic Response Control of Cantilevers Carrying Externally Mounted Stores," *Journal of the Acoustical Society of America*, Vol. 102, No. 6, Dec. 1997, pp. 3516–3522.
doi:10.1121/1.420397

[11] Na, S. S., and Librescu, L., "Optimal Dynamic Response Control of Adaptive Thin-Walled Cantilevers Carrying Heavy Stores and Exposed to Blast Pulses," *Journal of Intelligent Material Systems and Structures*, Vol. 11, No. 9, 2000, pp. 703–712.
doi:10.1177/104538900772663928

[12] Librescu, L., and Song, O., *Thin-Walled Composite Beams: Theory and Application*, Springer, New York, 2006, pp. 213–232, Chap. 8.

[13] Song, O., and Librescu, L., "Free Vibration of Anisotropic Composite Thin-Walled Beams of Closed Cross-Section Contour," *Journal of Sound and Vibration*, Vol. 167, No. 1, 1993, pp. 129–147.
doi:10.1006/jsvi.1993.1325

[14] Song, O., Ju, J. S., and Librescu, L., "Dynamic Response of Anisotropic Thin-Walled Beams to Blast and Harmonically Oscillating Loads," *International Journal of Impact Engineering*, Vol. 21, No. 8, 1998, pp. 663–682.
doi:10.1016/S0734-743X(98)00019-0

[15] Librescu, L., Meirovitch, L., and Song, O., "Refined Structural Modeling for Enhancing Vibrational and Aeroelastic Characteristics of Composite Aircraft Wings," *La Recherche Aerospatiale: Bulletin Bimestriel de l'Office National d'Etudes et de Recherches Aerospatiales*, Vol. 1, 1996, pp. 23–35.

[16] Rehfield, L. W., Atilgan, A. R., and Hodges, D. H., "Nonclassical Behavior of Thin-Walled Composite Beams with Closed Cross Sections," *Journal of the American Helicopter Society*, Vol. 35, No. 2, 1990, pp. 42–50.

[17] Librescu, L., *Elastostatics and Kinetics of Anisotropic and Heterogeneous Shell-Type Structures*, Noordhoff, Leyden, The Netherlands, 1975, pp. 406–407.

[18] Lee, I., and Lee, J-J., "Vibration Analyses of Composite Wing with Tip Mass Using Finite Elements," *Computers and Structures*, Vol. 47, No. 3, 1993, pp. 495–504.
doi:10.1016/0045-7949(93)90246-A

[19] Runyan, H. L., and Sewall, J. L., "Experimental Investigation of the Effects of Concentrated Weights on Flutter Characteristics of a Straight Cantilever Wing," NACA TN-1594, Nov. 1947.

[20] Qin, Z., and Librescu, L., "On a Shear-Deformable Theory of Anisotropic Thin-Walled Beams: Further Contribution and Validations," *Composite Structures*, Vol. 56, No. 4, 2002, pp. 345–358.
doi:10.1016/S0263-8223(02)00019-3

K. Shivakumar
Associate Editor